Accident Analysis and Prevention 82 (2015) 143–153

Contents lists available at ScienceDirect

Accident Analysis and Prevention

journal homepage: www.elsevier.com/locate/aap

Biofidelic neck influences head kinematics of parietal and occipital impacts following short falls in infants

Sarah Sullivan[a], Brittany Coats[b], Susan S. Margulies[a,*]

[a] Department of Bioengineering, University of Pennsylvania, Philadelphia, PA, United States
[b] Department of Mechanical Engineering, University of Utah, Salt Lake City, UT, United States

ARTICLE INFO

Article history:
Received 22 October 2014
Received in revised form 20 May 2015
Accepted 28 May 2015
Available online 11 June 2015

Keywords:
Pediatric traumatic brain injury
Biomechanics
Anthropomorphic test device

ABSTRACT

Falls are a major cause of traumatic head injury in children. Understanding head kinematics during low height falls is essential for evaluating injury risk and designing mitigating strategies. Typically, these measurements are made with commercial anthropomorphic infant surrogates, but these surrogates are designed based on adult biomechanical data. In this study, we improve upon the state-of-the-art anthropomorphic testing devices by incorporating new infant cadaver neck bending and tensile data. We then measure head kinematics following head-first falls onto 4 impact surfaces from 3 fall heights with occipital and parietal head impact locations. The biofidelic skull compliance and neck properties of the improved infant surrogate significantly influenced the measured kinematic loads, decreasing the measured impact force and peak angular accelerations, lowering the expected injury risk. Occipital and parietal impacts exhibited distinct kinematic responses in primary head rotation direction and the magnitude of the rotational velocities and accelerations, with larger angular velocities as the head rebounded after occipital impacts. Further evaluations of injury risk due to short falls should take into account the impact surface and head impact location, in addition to the fall height.

1. Introduction

From 2001 to 2012 falls were the leading cause of nonfatal injury to infants (≤1 year) and accounted for over 45% of all injuries in this age group (Melvin, 1995). Falls are also a commonly reported history in cases of suspected child abuse (Duhaime et al., 1987, 1992; Strait et al., 1995; Reece and Sege, 2000). Accurate biomechanical data can be used to predict diffuse brain injuries (e.g., traumatic axonal injury and intracranial hemorrhage), focal contusions, and skull fracture (Gennarelli et al., 1982; Raghupathi and Margulies, 2002; Yoganandan and Pintar, 2004; Delye et al., 2007; Monea et al., 2014). Therefore, a detailed understanding of the biomechanics of low height falls can help distinguish between accidental fall and abusive head injury etiologies.

Custom and commercially available infant anthropomorphic surrogates have been previously used to investigate the biomechanics of low height falls (Duhaime et al., 1987; Prange et al., 2003; Coats and Margulies, 2008; Thompson et al., 2009, 2013). However, the biofidelity of these surrogates was hindered by the paucity of infant neck tensile and bending stiffness data available at the time of their design. Neck designs in custom-made surrogates have included a hinge to represent a worst-case zero-resistance scenario (Prange et al., 2003), a naturalistic but not necessarily biofidelic rubber neck (Duhaime et al., 1987), and a rope-based neck that was validated against a single infant cadaver cervical spine motion segment (Coats and Margulies, 2008). The commercial CRABI series of pediatric surrogates have neck bending properties based on geometrically scaled down adult cadaver data, but do not take into account any other age-related differences in bending stiffness. They also lack specifications for tensile neck properties (Irwin and Mertz, 1997). With recent pediatric cadaver neck property data in tension and sagittal flexion/extension (Luck et al., 2008; Luck, 2012), we sought to improve the current "state-of-the-art" infant anthropomorphic surrogate design by creating a more biofidelic neck and better representing the properties of the intracranial contents. This surrogate was then used to measure the head kinematic response following falls onto a larger combination of impact surfaces, fall heights, and head impact locations than has been published previously. We analyze the influence of the biofidelic neck and head on the surrogate head kinematics by comparing results to those from our previous infant surrogate.

* Corresponding author at: 240 Skirkanich Hall, 210 South 33rd Street, Philadelphia, PA 19104-6321, United States. Tel.: +1 215 898 0882; fax: +1 215 573 2071.
E-mail address: margulie@seas.upenn.edu (S.S. Margulies).

http://dx.doi.org/10.1016/j.aap.2015.05.020
0001-4575/

2. Methods

2.1. Anthropomorphic surrogate weight and dimensions

The dimensions, weight distribution, body and limbs of a previously designed 1.5-month-old human infant anthropomorphic surrogate (Coats and Margulies, 2008) was used as the starting point for the new surrogate head and neck design. The surrogate's total head and body mass were matched to our previous surrogate (4.4 kg). The head mass was 1 kg, giving a head-to-body ratio of 0.23, which is consistent with the measurements reported by Duhaime et al. (1987) on 1-month-old infants. After completion, these weights approximately represented a 28th percentile male or 47th percentile female 1.5-month-old infant according to CDC Growth Charts (2000). Additional details on the anthropometry and development of the previous surrogate are reported elsewhere (Coats and Margulies, 2008).

2.2. Head and skull case

As previously developed (Coats and Margulies, 2008), the surrogate skull was composed of 5 copolymer polypropylene (Boston Brace International Inc.) plates attached together with silicone rubber (Smooth Sil 950, Smooth-On), and a 1-mm-thick latex cap was placed over the skull case to represent the scalp. The elastic modulus of copolymer polypropylene (535 ± 139 MPa, mean ± SD) was comparable to the elastic modulus of human parietal bone from infants aged 1–2 months old (518 ± 180 MPa). Similarly, the elastic modulus of silicone rubber (2.1 ± 0.2 MPa) was comparable to that of coronal suture from infants aged 40 weeks gestation to 1 month old (4.7 ± 1.5 MPa) (Coats and Margulies, 2006).

A triaxial angular velocity transducer with a bandwidth of 0.38–1000 Hz and linear acceleration sensitivity of less than 0.005 rad/s/g (ARS-06 Triaxial unit, ATA Sensors) was attached to a metal plate which extended rigidly from the top of the neck and was fixed in the center of the surrogate's head to measure sagittal, horizontal, and coronal angular velocities. The remaining space inside the skull case was filled with a linear viscoelastic silicone dielectric gel having a shear modulus of 765 ± 44 Pa, mean ± SD (Sylgard 527 A&B Silicone Dielectric Gel, Dow Corning, 1:1 A to B mix ratio) (Arbogast et al., 1997; Gefen and Margulies, 2004). This gel was used to represent human infant brain tissue, which was estimated to have a shear modulus of 559 Pa by scaling human adult brain properties by the adult-to-infant shear modulus ratio reported for piglet brain tissue (Prange and Margulies, 2002; Coats et al., 2007).

To validate the biofidelity of the surrogate head, the head construct was subjected to anterior–posterior (AP) and right-left (RL) parallel plate compression tests and compared to published infant (1–11 days old) cadaver head stiffness values (Prange et al., 2004). Mimicking the methods and data analysis used in the cadaver testing, the surrogate's head was compressed at fixed displacement rates of 0.05 mm/s and 1.0 mm/s to a total displacement of 5 mm in each loading direction. The stiffness was calculated as the slope of the force-displacement curve from 50% to 100% of the displacement target. The surrogate exhibited highly linear force–displacement characteristics over this range with R^2 values of 0.99–1, which match well with the reported R^2 values for the cadaver testing. At the quasistatic rate (0.05 mm/s), the surrogate and infant cadaver heads had similar compressive stiffness in both loading directions. At the higher rate, the infant cadaver was 4–5 times stiffer than the surrogate (Table 1).

Because the surrogate head had lower compressive stiffness at dynamic rates than the cadaver heads measured by Prange et al., an additional validation study was conducted to confirm that the peak impact forces measured by this surrogate were associated with incidence of skull fracture. To estimate conditions previously described by Weber (1984) for infant cadaver head drop experiments, we measured the peak impact force during a 91 cm (3 ft) fall onto concrete with an occipital–parietal impact location using a force plate described later in Section 2. Using the measured peak impact force as the input to a previously developed finite element model (FEM) of the infant head (Coats et al., 2007), we determined the peak maximum principal stress for each skull plate (left and right parietal and occipital). The probability of fracture for this peak principal stress was determined using published fracture risk curves based on the average infant parietal and occipital bone ultimate stress data (27 MPa and 9 MPa, respectively) (Coats and Margulies, 2006; Coats et al., 2007). The FEM-simulated peak maximum principal stress was 35.77 MPa in the parietal bone and 12.76 MPa in the occipital bone, which is associated with a 70% and 73% probability of fracture, respectively. This compares well with Weber's drop test results on $n = 5$ infant cadavers showing that 60% of the cadavers sustained occipital fractures and 80% had parietal fractures (Weber, 1984). We conclude after this detailed analysis that although the overall compressive stiffness of the head at dynamic rates is lower than Prange's compression results, the peak impact forces measured by the surrogate in an occipital–parietal impact event lead to realistic predictions of fracture. It should also be noted that Prange et al. reports the infant cadaver head was not rate-dependent between 1 and 50 mm/s. Therefore, any differences between the surrogate and cadaver head response are not likely to increase at higher rates.

Table 1
Compressive stiffness (average ± SD) from infant cadaver testing (Prange et al., 2004) and surrogate.

	Stiffness (N/mm)	
Direction—rate (mm/s)	Infant cadaver	Surrogate
AP—0.05	6.9 ± 2.4	4.2 ± 0.23
AP—1	20.8 ± 6.7	5.1 ± 0.29
RL—0.05	7.9 ± 1.6	4.5 ± 0.85
RL—1	25.7 ± 7.8	5.1 ± 0.32

AP = anterior–posterior compression, RL = right–left lateral compression.

2.3. Neck

The surrogate neck (Fig. 1) was constructed by molding a 2.54 cm diameter cylinder of Ecoflex 00-30 super soft silicone rubber (SmoothOn) with a length of Chemical Resistant clear Tygon Tubing (McMaster-Carr, 1.6 mm inner diameter, 4.8 mm outer diameter, 75A durometer rating) embedded in the center. This was then potted into two 3.8 cm-diameter plastic pipefittings using plaster, such that the flexible portion of the neck was 2.9 mm long. The silicone rubber allowed flexibility in all three rotational directions and the inner core of tubing dictated the tensile stiffness. To increase the bending stiffness in extension, three sets of double neoprene rubber bands were added along the ventrolateral surface of the neck (0.8 mm thick, 8 mm wide, 50A durometer rating).

The tensile properties of the surrogate neck were measured non-destructively by axially loading the neck at a fixed loading rate of 17 N/s up to a maximum load of 24 N for 5 separate trials. The mechanical response of the neck was linear ($R^2 = 0.995 \pm 0.002$), and the tensile stiffness was defined as the slope between 7 N and 15 N. This matched the loading range analyzed by Luck et al. The published tensile stiffness of a 24-day-old infant cadaveric osteoligamentous whole cervical spine and the surrogate neck were 7.3 N/mm and 5.5 ± 0.17 N/mm, respectively (Fig. 1) (Luck et al., 2008).

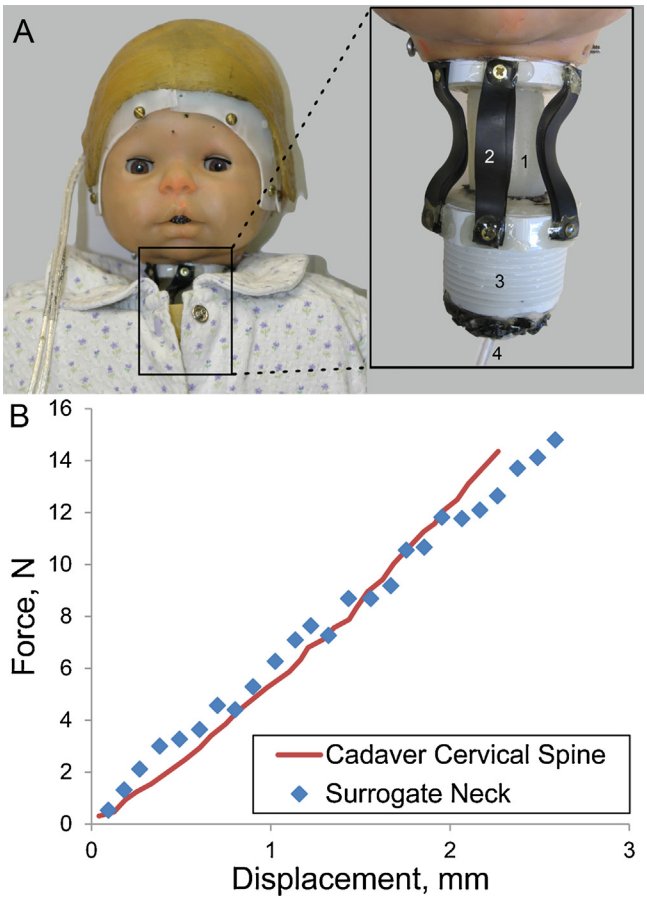

Fig. 1. (A) Anthropomorphic surrogate with improved neck biofidelity. The neck consisted of a silicone rubber body (1), double neoprene rubber bands to increase stiffness in extension (2), a threaded connector to attach to the body (3), and Tygon tubing molded into the center of the silicone rubber to increase the tensile stiffness (4). B) Force–displacement curve of the infant surrogate neck compared to infant (24-day-old) cadaver whole cervical spine (data digitized from Luck et al. (2008)).

The bending properties of the surrogate neck were measured by replicating the non-destructive bending tests performed by Luck (2012). The neck was quasistatically loaded to 0.07 Nm in flexion and 0.2 Nm in extension, which resulted in ~30° angular displacement in each direction. The resulting bending stiffness of the neck was 3.05 ± 0.23 mNm/° in flexion and 7.03 ± 0.28 mNm/° in extension. To compare the segmented spine cadaver data tested by Luck to the surrogate neck, the published stiffness function for each segment was evaluated at an age of 1.5 months old. An effective whole cervical spine stiffness, K_{eff}, was calculated using Eq. (1) by assuming each segment acted as a spring in series with other segments. K_i is the stiffness of each segment.

$$\frac{1}{K_{eff}} = \sum \frac{1}{K_i} \quad (1)$$

Not all cervical spine motion segments were tested by Luck et al. Therefore, a range of bending stiffness values were developed by first assuming that the missing motion segments had the same stiffness as the next lower tested segment, and then assuming that the missing segments were negligible to the effective response and eliminated from the series of spring. These assumptions yielded 2.6–4.3 mNm/° in flexion and 4.4–7.2 mNm/° in extension for the bending stiffness of a 1.5-month-old infant whole cervical spine. The surrogate bending stiffness values fall within these estimated ranges. The surrogate neck was not tested in lateral flexion/extension or axial torsion as no pediatric human data is available for validation.

2.4. Drop testing protocol

The instrumented infant anthropomorphic surrogate underwent a series of headfirst drop tests from 3 heights (30 cm (1 ft), 61 cm (2 ft), 91 cm (3 ft)) onto 4 surfaces (concrete, wood laminate, carpet with carpet pad, and crib mattress) with two head impact locations (occipital and parietal).

The laminate wood sample was constructed from 1.1-cm-thick self-locking planks with 1-mm-thick underlayment attached (Academy Floor), which was then glued to a plywood base (1.8 cm thick), simulating the subfloor. The carpet and carpet pad were each 0.6 cm thick. The crib mattress was 15 cm thick with an innerspring structure, and its material properties have been described in detail previously (Coats and Margulies, 2008). All impact surfaces were clamped to a six degree of freedom force plate (Model FP4060-07, Bertec).

To evaluate a worst-case scenario, where the head impact is undiluted by previous or simultaneous contact with other body regions, the surrogate was positioned such that there was a clear head impact before any portion of the surrogate's body began to impact. This type of event mimics a head-first fall from a table or couch where the head impacts the floor unimpeded, without the arms or other body parts "braking" the fall. The neck was placed in a neutral position by aligning the ears of the head with the shoulders and centering the nose and chin with the body. Panel A of Figs. 2 and 3 depict the initial surrogate positions, where the entire body was angled, with the head pointing downward, at approximately 20° for occipital impacts (see also photograph in our previous publication (Coats and Margulies, 2008)) and 30° for parietal impacts. The initial body position was angled more sharply for parietal impacts so that the head impacted before the shoulder. If the body were angled to the same degree for occipital impacts, the impact location would no longer be on the occiput, but rather the posterior fontanel or along the sagittal suture. High-speed digital video (210 fps, Exilim EX-FC100, Casio) was used to verify a head first impact and to observe the kinematic response of the surrogate for the first few drops of each impact location. Care was taken to replicate the surrogate positioning on all drop tests.

Ten drops were conducted for each combination of height, impact surface, and head impact location, resulting in a total of 240 drops. After every 5 drops the skull assembly was replaced and the doll's head re-packed in order to incorporate uncontrolled variation in skull assembly construction and head packing into the measurements. The surrogate neck was routinely checked for damage. Damaged necks were replaced by new neck constructs. All neck constructs were tested prior to use to ensure a <10% variation in tensile and bending stiffness.

2.5. Data analysis

Angular velocity in three directions and normal impact force were collected at 10,000 Hz using a data acquisition system (Labview, National Instruments). Angular velocities were cropped to include the first full head rotation. The signal processing standard, SAE J211 specifies a fixed value, low-pass cutoff of 1 kHz for head accelerations of occupant surrogates in road vehicle impact tests. Because accelerations resulting from road vehicle impacts are often at higher rates than those resulting from short falls, we conducted a spectral analysis on each angular velocity trace and used the corner frequency of the power spectral density to define an impact specific cutoff frequency, which ranged from 83 Hz (mattress impacts) to 1760 Hz (concrete impacts). Using the impact specific cutoff frequency, the velocity traces were filtered

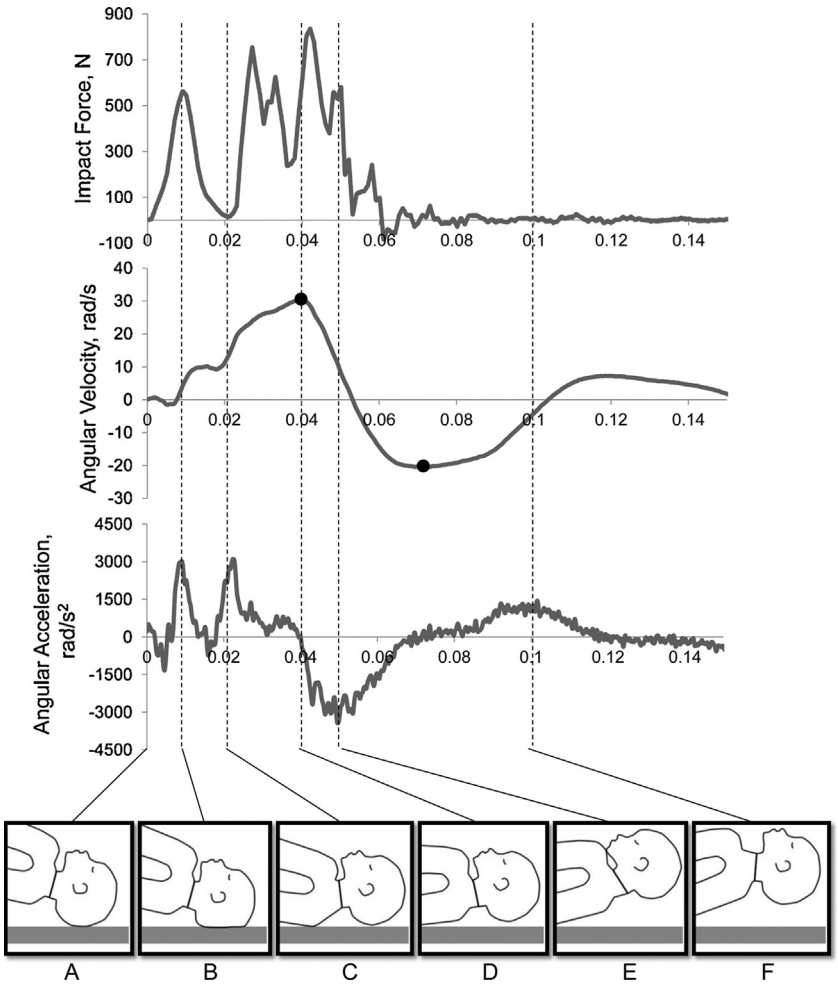

Fig. 2. Example force, sagittal angular velocity, sagittal angular acceleration traces, and corresponding surrogate position in response to a 61 cm (2 ft) drop onto concrete with occipital impact (845 Hz cutoff frequency). (A) Surrogate position the moment before impact. (B) The point of peak head impact force corresponds with first peak in angular acceleration and is clearly distinguishable from body impact force. (C) The point where the body begins to impact, also causing the second peak in angular acceleration. (D) The point of peak angular velocity as the head is rotating toward the chest. Black dots indicate points of peak-to-peak change in velocity. (E) The peak angular deceleration occurs when the chin hits the chest. (F) The position of the head after it has rebounded from impact with chest and is fully rotated toward the back.

with a 4th order, low-pass Butterworth filter. The filtered angular velocity data were differentiated to obtain angular acceleration. The peak angular acceleration and the largest peak-to-peak change in angular velocity (indicated by black dots on Figs. 2 and 3) were extracted from the sagittal, coronal, and horizontal rotational directions for further analysis. A resultant peak angular velocity and acceleration was also calculated. Impact force data were not filtered.

Peak head impact force was easily identified and extracted from the force-time signal (panel B of Figs. 2 and 3), except for impacts onto the crib mattress. The mattress was so compliant that the head did not begin to rebound before the body impacted, making it impossible to extract an accurate reading for isolated head impact forces on that surface. The overall peak force was extracted in these cases with the caveat that they would overestimate the force experienced by the head. The duration of head impact was defined as the non-zero force interval from head impact to head lift-off. In cases when the body impacted before head lift off, the time duration between head impact and peak force was extracted and doubled. Impact durations for falls onto the crib mattress were not calculated due to the reasons stated above.

Two-way ANOVAs with height and impact surface as the main effects were conducted for each impact location to evaluate significant differences in peak angular acceleration, peak-to-peak angular velocity, impact force, and impact duration. Tukey–Kramer post-hoc testing was performed to determine significance among groups within each main effect. Distributions of the kinematic measurements were not normally distributed, so data was rank-transformed prior to analysis. Statistical significance was set at $p < 0.05$.

3. Results

Fall direction affects the timing of the head kinematics. In occipital impacts (Fig. 2), the head rotates slightly as it impacts the plate, resulting in a small negative angular velocity between points A and B. As impact continues with increasing linear acceleration and impact force, head rotation slows during deformation at impact. Then the head rolls at the point of impact, reversing head rotation direction and increasing velocity and acceleration before peak impact force at B. As the head rebounds after B, lifting off the plate by C, impact force decreases and velocity plateaus, until the thorax impacts at C (0.2 s), causing a sharp increase in the head's rebound angular velocity and acceleration. The flatter surface of the head and larger lateral flexion at shoulder contact during parietal impacts (note larger negative velocity peak before B in Fig. 3 than Fig. 2) alters the kinematics between head contact and rebound from the surface (B and C). The flatter head surface

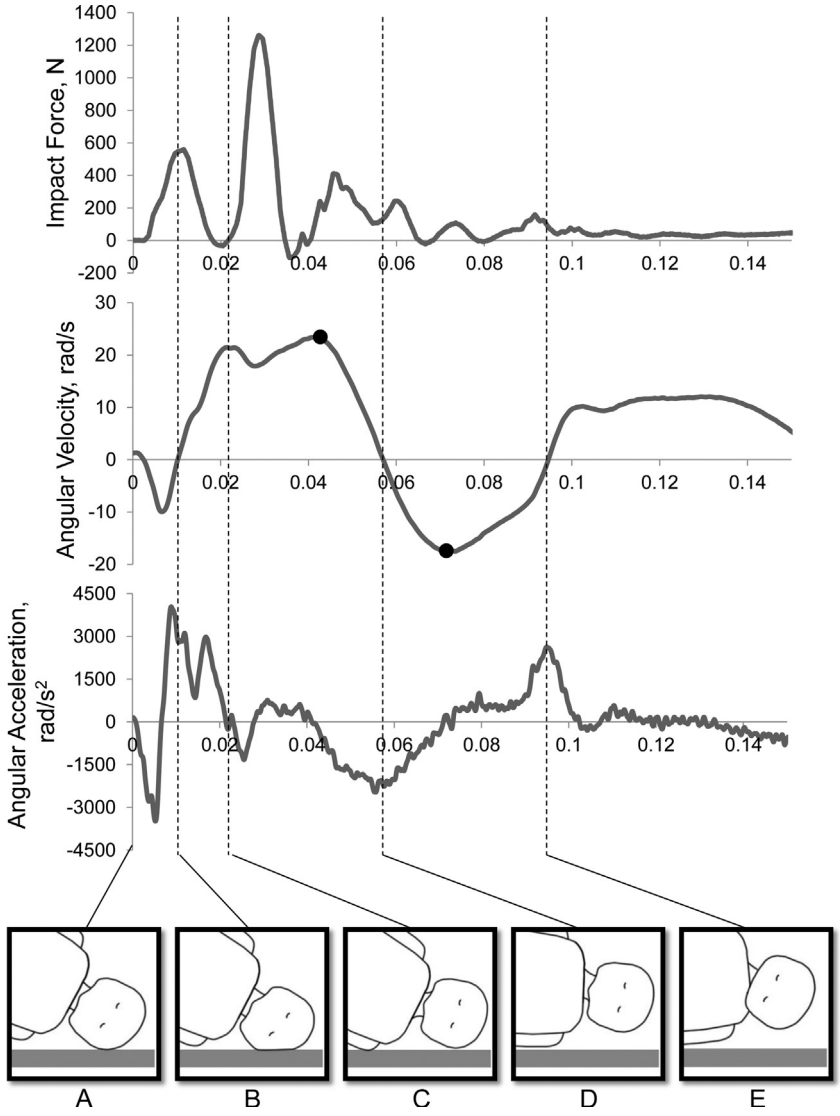

Fig. 3. Example force, coronal angular velocity, coronal angular acceleration traces, and corresponding surrogate position in response to 61 cm (2 ft) drop onto concrete with parietal impact (734 Hz cutoff frequency). (A) Surrogate position the moment before impact. (B) The point of peak head impact force corresponds with peak in angular acceleration and is clearly distinguishable from body impact force. (C) The moment the body impact begins as the head is rotating counterclockwise at almost the peak angular velocity. Black dots indicate points of peak-to-peak change in velocity. (D) The head reaches its maximum rotational excursion, but it does not impact the opposing shoulder. (E) The head rotates back clockwise, and the chin rolls into the chest, resulting in a large sagittal angular velocity (sagittal trace not shown).

increases contact friction and reduces rolling during impact, shortening the velocity plateau. Because the neck has little resistance to lateral bending, rebound rotation is hastened, with velocity peaking as the head lifts off the plate at C, and again as the shoulder impacts between C and D. Below, the values of peak impact force, acceleration, and velocity are compared across drop height and direction.

3.1. Peak impact force and duration

Peak head impact force significantly increased ($p < 0.0001$) and impact duration significantly decreased ($p < 0.0001$) at greater drop heights for both occipital and parietal impact locations (Fig. 4 and Tables 2 and 3). Peak impact forces were similar for both parietal and occipital impact locations at each drop height. The impact duration for parietal falls was greater than occipital falls, but only at 30 cm. The largest mean head impact forces for parietal and occipital impact locations were 621 and 592 N, respectively, and occurred during the 91 cm drops onto concrete.

The peak head impact force and duration was significantly influenced by the impact surface ($p < 0.0001$). Head impact forces on mattress were significantly lower than all other impact surfaces in both impact locations despite the fact that the force measurements for this surface were an overestimation of the actual head impact force ($p < 0.0001$). The impact force was significantly lower on carpet than concrete ($p < 0.005$), but there were no significant differences between concrete and hardwood laminate for both impact locations (Table 2). Impact force duration followed inverse trends to impact force. Duration was greatest for carpet, and not significantly different between laminate and concrete for occipital falls. Parietal falls were slightly different as laminate had significantly larger impact durations ($p < 0.0001$) than concrete at 30 and 61 cm.

3.2. Peak angular acceleration

The drop impact location strongly influenced which head rotational directions had the highest peak angular accelerations (Fig. 5). As expected, peak accelerations from occipital impacts

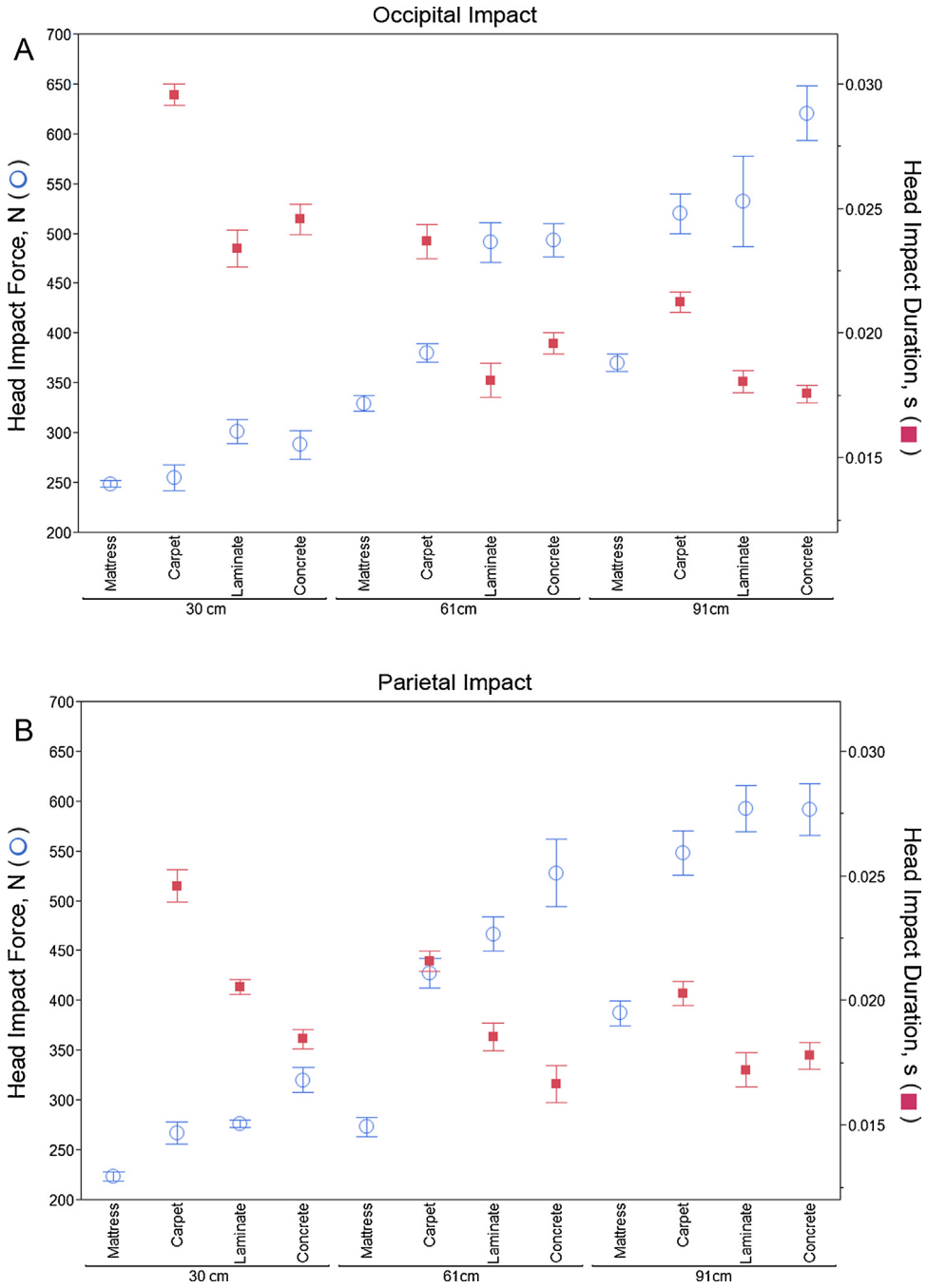

Fig. 4. Peak head impact forces and durations for occipital (A) and parietal (B) impacts from 30 cm (1 ft), 61 cm (2 ft), and 91 cm (3 ft) onto different surfaces. It was impossible to isolate a head impact force and duration for impacts onto the crib mattress. The overall peak force is plotted here for mattress impacts. This is an overestimate of the force experienced by the head. Mean ± standard error.

were greatest in the sagittal direction followed by the coronal and lastly the horizontal direction. On average, sagittal accelerations were 2.4 times higher than coronal and coronal were 2 times higher than horizontal. For parietal impacts, the average peak accelerations were the largest in the coronal and sagittal directions, which had approximately the same magnitude (coronal: 2830 rad/s^2; sagittal: 2424 rad/s^2). Peak accelerations in the horizontal plane were 4.6–5.4 times lower than the accelerations in the other two planes.

Peak head angular acceleration in each rotational direction and the resultant acceleration were significantly affected by drop height for both impact locations ($p < 0.005$, Fig. 5). For occipital impacts, peak accelerations were significantly higher following 91 cm drops than 30 cm drops ($p < 0.002$, Table 2), but there was no significant difference in resultant peak acceleration between 91 cm drops and 61 cm drops. However, for parietal impacts, drops from 91 cm resulted in significantly larger peak accelerations than those from 61 cm, which in turn were significantly larger than those from 30 cm for all directions, and the resultant value ($p < 0.009$, Table 3).

For occipital impacts, there was a significant effect of impact surface on angular acceleration in each rotational direction and on the resultant acceleration ($p < 0.0001$). Concrete, laminate hardwood, and carpet had significantly higher peak angular accelerations than mattress ($p < 0.0001$, Table 2). However, there were no significant differences between carpet and concrete. In contrast, for parietal impacts, the concrete and laminate had significantly

Table 2
Occipital impact statistical comparisons for all measurements.

		Impact		Angular acceleration				Pk–Pk angular velocity			
		Force	Duration	Sag	Cor	Hor	Res	Sag	Cor	Hor	Res
Height	30 cm	A	A	A	A	A	A	A	A	A	A
	61 cm	B	B	B	B	A B	B		B	A	
								B			B
	91 cm		C		B	B	B		B	A	
		C		C				B			B
Impact surface	Mattress	A	–	A	A	A	A	A	A	A	A
	Carpet	B	B	B	B	B	B	B	B	B	B
	Laminate		C	B				B			B
		C			C	C	C		C	C	
	Concrete		C	B	B C	B C	B C	B	B C	B C	B
		C									

Levels connected by the same letter were not significantly different. Sag = sagittal, Cor = coronal, Hor = horizontal, Res = resultant.

Table 3
Parietal impact statistical comparisons for all measurements.

		Impact		Angular acceleration				Pk–Pk angular velocity			
		Force	Duration	Sag	Cor	Hor	Res	Sag	Cor	Hor	Res
Height	30 cm	A	A	A	A	A	A	A	A	A	A
	61 cm	B	B	B	B	B	B	B		A	B
									B		
	91 cm	C	B							B	
				C	C	C	C	C	B		C
Impact surface	Mattress	A	–	A	A	A	A	A	A	A	A
	Carpet	B	B	B	B	B	B	B	B	B	B
	Laminate	B C	C				C	B	B	B	
				C	C	C					C
	Concrete		D				C	B	B	B	B C
		C		C	C	C					

Levels connected by the same letter were not significantly different. Sag = sagittal, Cor = coronal, Hor = horizontal, Res = resultant.

higher peak accelerations than carpet, which in turn had significantly higher peak accelerations than the crib mattress ($p < 0.01$).

3.3. Peak-to-peak change in angular velocity

The drop impact location highly influenced the direction of the head rotational response, represented by the peak-to-peak change (pk–pk) in angular velocity (Fig. 6). Not surprisingly, for occipital impacts, the change in velocity was the largest in the sagittal direction, followed by the coronal direction, and lastly, the horizontal direction. On average, sagittal pk–pk velocity was 3.5 times higher than coronal, and coronal was 2.6 times higher than horizontal. In contrast, parietal impacts had the highest pk–pk velocity in the coronal direction, which was then followed closely by the sagittal direction. The horizontal direction once again had the smallest pk–pk velocities. The average change in velocity was only 1.5 times higher in the coronal direction than the sagittal direction, but was 3.8 times higher in the sagittal direction than the horizontal direction.

For occipital impacts, the pk–pk velocity was significantly affected by drop height in the sagittal and coronal rotational planes ($p < 0.001$), but not the horizontal (Table 2). The peak resultant velocity was also significantly affected by drop height ($p < 0.0001$). The 91 cm and 61 cm falls had significantly higher peak resultant angular velocities than 30 cm ($p < 0.01$), but they did not have significantly different angular velocities from each other (Table 2).

In contrast, the peak resultant velocity for parietal impacts was significantly higher following drops from 91 cm than 61 cm ($p < 0.002$), which in turn had significantly higher velocity than 30 cm drops ($p < 0.0001$). There were also significant effects of drop height on the pk–pk angular velocity in all three rotational directions with a parietal impact location unlike occipital impacts ($p < 0.0001$, Table 3).

Impact surface significantly affected pk–pk and peak resultant angular velocity for both occipital and parietal impacts; crib mattress impacts exhibited significantly lower angular velocities than any of the other impact surfaces in each rotational direction and in the resultant value ($p < 0.002$). However, the angular velocity was not significantly different following carpet and concrete impacts for any rotational direction or impact location.

4. Discussion

4.1. Effect of head and neck design: comparison to previously published surrogate data

The surrogate created in this study builds upon a previous surrogate (Coats and Margulies, 2008) that was used to measure the kinematics of low height falls with occipital impacts onto three surfaces (mattress, carpet pad, and concrete). The surrogate enhancements include (1) a more biofidelic neck based upon recent tensile and bending properties reported for cadaver infants, (2) intracranial material with a shear modulus similar to brain tissue, and (3) advanced instrumentation that directly measures three-dimensional angular velocity and impact force. This enhanced design was then used to investigate additional impact surfaces (mattress, carpet and carpet pad, laminate hardwood, concrete) and two different locations of head impact (occipital, parietal).

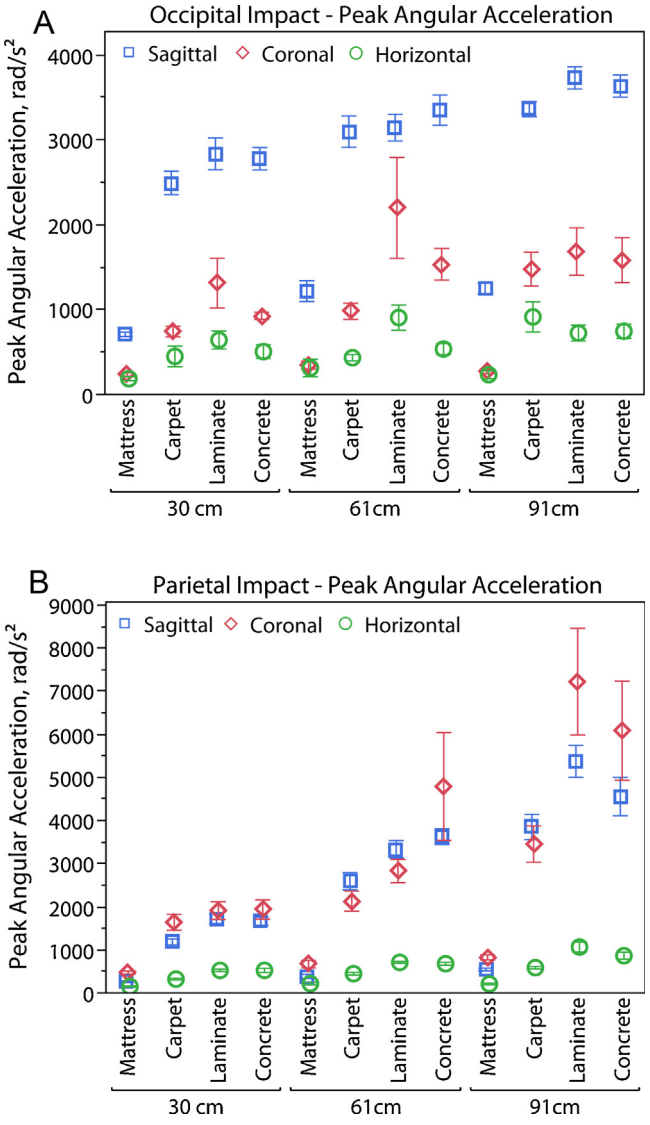

Fig. 5. Peak angular acceleration for occipital (A) and parietal (B) impacts from 30 cm (1 ft), 61 cm (2 ft), and 91 cm (3 ft) onto different surfaces. Mean ± standard error.

Comparing the occipital impacts onto concrete from the present study to those published with the previous surrogate, we found that impact forces, angular accelerations, and velocities were generally lower in the more biofidelic surrogate. The range of impact forces in the present study ranged from 288 N at 30 cm to 621 N at 91 cm, while the previous impact forces ranged from 316 N at 30 cm to 1324 N at 91 cm. Correspondingly, the range of sagittal plane angular accelerations and velocities from the previous study were 4500–16,596 rad/s^2 and 21–115 rad/s, respectively, while the range of sagittal plane angular accelerations and velocities for the present study were 2777–3632 rad/s^2 and 44–49 rad/s, respectively. The changes in the surrogate neck alone do not explain the measured differences in angular acceleration and velocity from our previous surrogate. The increased biofidelity of the neck decreased the overall sagittal plane bending stiffness by approximately 2.2 times in flexion and 3.6 times in extension. Intuitively, this decrease in stiffness would have increased the angular acceleration and velocity of the head. Therefore, we conclude that the overall decrease in the kinematic parameters was overshadowed by the increased compliance of the head and possibly variations in the starting position of the surrogate.

The peak impact force was also influenced most by the change in compliance of the head. The previous surrogate had larger intracranial instrumentation and required that packets of lead balls be secured inside the head to reach the appropriate head mass. In the present study, the intracranial instrumentation had a smaller footprint and a silicone gel with shear properties similar to brain tissue was used to fill the void. This resulted in an overall more compliant head in the updated surrogate that increased the time of deceleration upon impact and lowered impact forces. The shear modulus of the silicone gel was slightly higher than the estimated shear modulus for infant brain (765 Pa vs. 559 Pa). Based on parametric finite element simulations of infant head impact (Coats et al., 2007), this increased shear modulus may increase impact forces by 3.5% and decrease impact durations by 2%. This change would alter our largest force measurement (621 N) by 22 N. However, this slight overestimation may be beneficial by compensating for the slightly lower compliance of the surrogate head at dynamic rates compared to cadaver studies.

In addition to head compliance, the initial positioning of the surrogate could contribute to changes in the head impact kinematics between the two studies. In the present study, the head and body were kept in line and angled downward together (as depicted in Panel A in Figs. 2 and 3), which likely decreased head rebound compared to the previous surrogate study which positioned the surrogate supine with only the head angled downward. The head impact force peaked during a period when only the head was in contact with the ground (Figs. 2 and 3), and did not substantially differ between parietal and occipital impacts. The orientation of the body, therefore, does not appear to substantially influence peak impact force. This is supported further by a similarity in our measurements of peak occipital head impact force (295 ± 42 N) to the impact force measured in a single infant cadaver head with no body or neck (336 N) reported by Prange et al. (2004). However, the average contact duration in our studies (0.024 ± 0.002 s) was greater than that reported by Prange (0.020 s). This was likely due to the presence of a neck and body in our study. The neck tethers the head to the torso, which is continuing to move downward while the head is trying to rebound upward. The head kinematics are therefore substantially affected by the positioning of the entire multicomponent system from this point forward. In fact, the peak angular velocity of both occipital and parietal impacts in the present study occurred after the body impact (Figs. 2 and 3). The peak angular acceleration occurred after the body contacted the flooring for occipital impacts, but prior to body contact for parietal impacts. Prior surrogate studies (Duhaime et al., 1987; Prange et al., 2003; Coats and Margulies, 2008) and the present study all agree that the neck and body have a substantial effect on the head kinematics, and needs to be carefully considered in biomechanical analysis.

One important difference between the two studies was the resulting head rotation direction following an occipital impact. In the prior study, head rotations in the sagittal and horizontal planes equally dominated the kinematic response (10,633 rad/s^2 and 8048 rad/s^2, respectively, for 61 cm fall onto concrete). In this study, sagittal head rotations were more dominant than horizontal rotations following an occipital impact (3348 rad/s^2 and 536 rad/s^2, respectively, for 61 cm fall onto concrete). There are two factors that likely contribute to this change. First, whereas sagittal angular accelerations were measured directly in both models, the horizontal and coronal angular accelerations were calculated in the previous surrogate. The horizontal calculations tended to overestimate measured values. Second, the previous design used a twisted rope as the base of the neck and may have been predisposed to horizontal rotations. The current neck design was created with Tygon tubing surrounded by a solid silicone rubber body. There is currently no information on the torsional

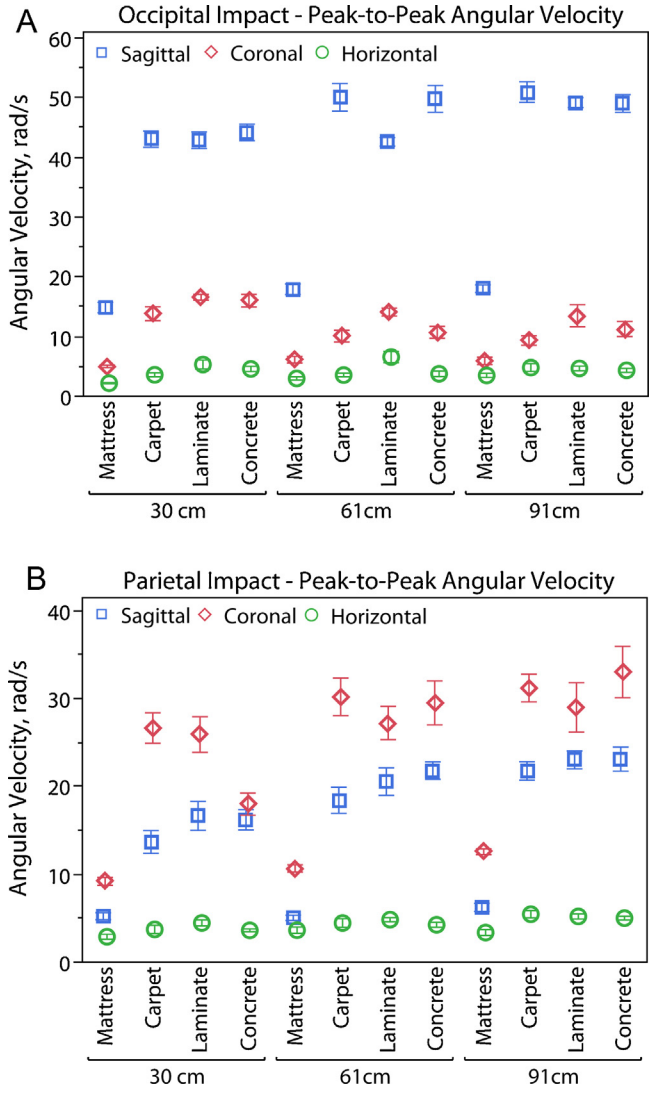

Fig. 6. Peak-to-peak angular velocities for occipital (A) and parietal (B) impacts from 30 cm (1 ft), 61 cm (2 ft), and 91 cm (3 ft) onto different surfaces. Mean ± standard error.

properties of the infant neck, so we are unable to determine appropriate design parameters for torsional stiffness.

4.2. Effect of head impact location

Our goal was to evaluate a worst-case scenario, where the head impact is unimpeded by previous or simultaneous contact with other body regions. As such, the surrogate starting position was angled approximately 20° for occipital impacts and 30° for parietal impacts as illustrated in panel A of Figs. 2 and 3. The larger angle for parietal impacts was necessary so that the head impacted before the shoulder. If this larger angle was used for occipital impacts, the impact location would no longer be on the occipital prominence, but rather on the posterior fontanel or along the sagittal suture. Our surrogate positioning was successful in producing similar head impact forces for parietal and occipital headfirst impacts. However, peak angular accelerations and velocities that occurred as a result of those impact forces were different between parietal and occipital head impacts. The peak resultant angular acceleration after a parietal impact increased more sharply with increases in impact force than after an occipital impact (Fig. 7A and B), perhaps due to its steeper initial angle of inclination. For example, 91 cm

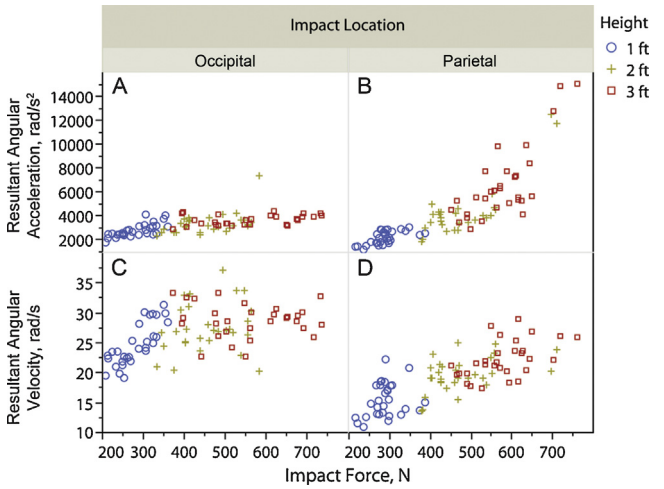

Fig. 7. Impact force vs. peak resultant angular acceleration and peak resultant angular velocity with each carpet, hardwood laminate, and concrete drop represented as one data point. Drops onto mattress are not included here due to limitations for measuring the head impact force precisely.

(3 ft) falls with parietal impacts onto concrete had a much greater average resultant peak angular acceleration (6962 rad/s^2) than occipital impacts (3693 rad/s^2). The peak resultant angular velocity, however, was overall higher after an occipital impact than a parietal impact (Fig. 7C and D). It is worth noting that the peak angular acceleration primarily occurs during the impact event, while the peak angular velocity occurs during the rebound (Figs. 2 and 3). Again, these differences may be associated with the initial angles of inclination.

Not surprisingly, the occipital impacts resulted in angular velocities and accelerations primarily in the sagittal plane, with much smaller velocities and accelerations in the coronal and horizontal planes. Parietal impacts began with head rotations primarily in the coronal plane, as anticipated, but after this initial coronal rotation the head then rolled in the sagittal plane towards the chest.

There is broad agreement in the literature that impact location and the subsequent rotational direction of the head plays an important role in the development and severity of injury. Both the magnitude of the inertial response (velocity and acceleration) and the relative direction-specific vulnerability of the brain tissue injury response contribute to injury outcomes in children and adults. Pellman and colleagues reconstructed game impacts of concussed professional football players with Hybrid III test dummies and found that significantly lower peak head accelerations resulted in concussion when the impact was to the facemask than when the impact was to other parts of the helmet shell (Pellman et al., 2003). Broglio et al. (2010) measured head impact kinematics in high school football players both with and without resulting concussion. Impacts to the front and back of the helmet, as well as impacts to the top of the helmet, more commonly resulted in concussion. Similar to these human studies, sagittal head rotations in immature piglets have been shown to result in overall worse outcomes. The Margulies Lab reports longer durations of unconsciousness, larger decreases in cerebral blood flow, greater behavioral changes, and more persistent axonal injury following sagittal head rotation compared to other rotational directions (Eucker et al., 2011; Sullivan et al., 2013). However, TBI studies in adult primates report that coma and diffuse axonal injury was more severe after coronal plane head rotations (Gennarelli et al., 1982). Furthermore, a finite element model analysis of the effect of head rotation direction on strain reported that human head rotations in the horizontal plane

resulted in the largest distribution of high strains (Weaver et al., 2012). These data highlight the importance of head rotation direction on outcome, but disagreement among the conclusions suggests more research is needed to determine direction-specific thresholds for traumatic brain injury.

4.3. Effect of height and surface

As expected based on other epidemiology and biomechanical studies (Coats and Margulies, 2008; Haney et al., 2010; Ibrahim and Margulies, 2010; Thompson et al., 2011), we found that higher falls (91 cm or 3 ft) significantly increased impact force, peak angular acceleration, and peak resultant angular velocity for both impact locations when compared to 30 cm (1 ft). Impacts onto concrete or laminate hardwood produced similar kinematics, which were higher than impacts onto crib mattress. Falls onto carpet had significantly lower peak impact forces than concrete for both occipital and parietal impacts, and they had significantly lower peak angular accelerations in all rotational directions for parietal impacts. However, angular velocity following a fall onto carpet did not differ significantly from concrete.

4.4. Injury risk

Much effort has been made to determine kinematic thresholds for head injury based on primate head injury studies (Duhaime et al., 1987; Margulies and Thibault, 1992; Ommaya et al., 2002), human cadaver experiments (Depreitere et al., 2006), and injuries reported in helmet-instrumented football players (Broglio et al., 2010; Rowson et al., 2012). Developmental changes in physiology, anthropometry, and brain tissue mechanical properties make it impractical to use these thresholds for the prediction of head injury in an infant. Furthermore, the rotational direction of the head following impact is an important component in the severity of injury; however, published head injury thresholds do not take into account head rotation direction, but rather attempt to provide a single cutoff value for injury regardless of the impact location and subsequent rotational direction. Epidemiological studies investigating injuries from low height falls provide useful insight into the trends of injury, but statistical groupings span several ages (e.g., 0–5 years old), several heights (e.g., 0–5 feet) and multiple types of falls (e.g., head first, feet first, parietal impact, occipital impact, etc.). It is therefore impractical to determine probabilities of injury on a case-by-case basis using this data.

With these limitations in mind, we decided to compare the loads from the low height falls in the present study to published kinematic thresholds and existing epidemiology data solely as a qualitative assessment of injury risk. The threshold for concussion scaled to infant brain mass (400 g) has been proposed to be between 10,000 and 15,000 rad/s^2 peak angular acceleration based on adult primate data (Duhaime et al., 1987; Ommaya et al., 2002) and instrumented football helmet data, respectively (Broglio et al., 2010; Rowson et al., 2012). No resultant acceleration for any occipital impact fall exceeded this lower bound. For parietal impacts, the lower bound was exceeded for 2/10 falls from 61 cm (2 ft) onto concrete, 1/10 falls from 91 cm onto concrete, and 2/10 falls from 91 cm onto hardwood laminate. The higher bound of 15,000 rad/s^2 was exceeded only for one 91 cm fall onto concrete (peak angular acceleration of 15,085 rad/s^2). When averaging across all fall trials for a fall height, impact surface, and impact location, none of these average peak angular accelerations exceeded the 10,000 rad/s^2 concussion threshold lower bound. Mayr et al. (1999) reported 13.6% of children (7–30 months old; mean = 13 months) experienced a concussion following a fall from a highchair. Tarantino et al. (1999) reported 11% of 167 children (<10 months old) experienced a closed head injury following a <4 ft fall. These statistics are comparable to the percentage of parietal 3 ft falls detailed above that exceeded the lower threshold (3 out of 20, or 15%).

Thresholds for subdural hemorrhage (SDH) have been proposed to be between 10,000 and 35,000 rad/s^2 based on adult human cadaver impacts (Depreitere et al., 2006) and primate data (Duhaime et al., 1987), respectively. As stated above, although a few 61–91 cm falls onto concrete or hardwood laminate had peak angular accelerations in excess of the 10,000 rad/s^2 subdural hemorrhage threshold, none of the average peak angular accelerations exceeded 10,000 rad/s^2 and not a single trial had a peak angular acceleration greater than or equal to 35,000 rad/s^2. The presence of subdural hemorrhages in low height falls of infants is noticeably absent in the epidemiological fall literature. Thompson et al. (2011) reported 2 subdural hematomas in 79 falls in children <4 years old. The cases involved a 42 month old and 1 month old child. The one-month old child was sleeping on his mother's chest and rolled over, striking his head on a humidifier before falling 0.89 m onto the ground. Assuming the lower threshold for concussion is the same as for SDH, we would again predict SDH in 15% of our 3 ft parietal falls onto hard surfaces. However, based on the comparison with the epidemiology literature, it is likely that this lower SDH threshold is inaccurate.

Specific impact force tolerances for pediatric skull fracture have not been published, and scaling fracture tolerances from adult studies is unrealistic given the distinct differences in cranial bone structure between children and adults. Helfer et al. (1977) reported 2 skull fractures in 161 children <5 years old that fell from a bed or sofa. Both children were under 2 years old. Mayr et al. (1999) reports 16% of 103 children 7–30 months experienced a skull fracture following a fall from a highchair. Tarantino et al. (1999) reported 17% of 167 infants <10 months old had a skull fracture in falls <4 ft. Future work will incorporate the fall kinematic data in this study with published pediatric skull ultimate stress data (Coats and Margulies, 2006) to develop risk curves for skull fracture.

While this surrogate significantly advances the state of the art in ATDs by increasing the biofidelity of the neck, there are still two limitations of the surrogate. First, although the bending stiffness of the surrogate's neck was obtained quasistatically, and is in the range of published values (Luck, 2012; Luck et al., 2008), it is possible that because the surrogate neck bending stiffness was at the low end of the derived range for flexion and the high end of the derived range for extension, the exaggerated flexion–extension difference could influence the measured kinematics, particularly for occipital impacts. Second, the infant neck properties in lateral bending and torsion are unknown and thus, not validated in this design. With occipital impacts, the primary direction of rotation was sagittal (anterior–posterior) and would be affected minimally by lateral and torsional stiffness. Impacts to the parietal skull resulted in both coronal and sagittal rotation. We speculate that coronal rotation would be influenced most by lateral neck bending properties. The torsional stiffness would affect the twisting of the head toward the chest, and subsequent sagittal rotation, as described earlier.

In summary, this study presents the kinematics of short falls using a biofidelic infant surrogate with improved neck bending and tensile properties designed to mimic recently published infant cadaver properties, with intracranial contents matched to the shear modulus of brain tissue, and with advanced instrumentation to directly measure three-dimensional angular velocities and impact force. Skull compliance, neck bending, and tensile properties significantly influenced the measured kinematic loads. By increasing the skull compliance, the impact force and peak angular acceleration were substantially decreased from previously published results, lowering the expected injury risk. While more

compliant impact surface materials (e.g., crib mattress versus concrete) and lower fall heights reduce kinematic responses as we have reported previously, herein we now report that occipital and parietal impacts have distinct kinematic responses both in terms of the direction of head rotation and the magnitude of the rotational velocities and accelerations, and greater response to variations in fall height and impact surface stiffness. These direction-specific kinematic data will become critical to identifying probabilities of injuries from low height falls in children when pediatric injury threshold data becomes available.

Conflict of interest

Dr. Margulies reports grants from the Centers for Disease Control and Prevention and the National Institutes of Health during the execution of the study; there are no other known conflicts of interest.

Acknowledgments

We gratefully acknowledge Megan Weil for her assistance in conducting the drop tests. This study was made possible by the Centers for Disease Control and Prevention grant NCIPC R49CE000411 and the National Institutes of Health (NIH)/National Institute of Neurological Disorders and Stroke (NINDS) grant R01NS039679.

References

Arbogast, K.B., Thibault, K.L., Pinheiro, B.S., Winey, K.I., Margulies, S.S., 1997. A high-frequency shear device for testing soft biological tissues. J. Biomech. 30 (7), 757–759.

Broglio, S.P., Schnebel, B., Sosnoff, J.J., Shin, S., Feng, X.D., He, X.M., Zimmerman, J., 2010. Biomechanical properties of concussions in high school football. Med. Sci. Sports Exercise 42 (11), 2064–2071.

CDC Growth Charts, 2000. Centers for Disease Control and Prevention. National Center for Health Statistics, United States.

Coats, B., Margulies, S.S., 2006. Material properties of human infant skull and suture at high rates. J. Neurotrauma 23 (8), 1222–1232.

Coats, B., Margulies, S.S., Ji, S., 2007. Parametric study of head impact in the infant. Stapp Car Crash J. 51, 1–15.

Coats, B., Margulies, S.S., 2008. Potential for head injuries in infants from low-height falls. J. Neurosurg. Pediatr. 2 (5), 321–330.

Delye, H., Verschueren, P., Depreitere, B., Verpoest, I., Berckmans, D., Vander Sloten, J., Van Der Perre, G., Goffin, J., 2007. Biomechanics of frontal skull fracture. J. Neurotrauma 24 (10), 1576–1586.

Depreitere, B., Van Lierde, C., Sloten, J.V., Van Audekercke, R., Van der Perre, G., Plets, C., Goffin, J., 2006. Mechanics of acute subdural hematomas resulting from bridging vein rupture. J. Neurosurg. 104 (6), 950–956.

Duhaime, A., Gennarelli, T., Thibault, L., Bruce, D., Margulies, S., Wiser, R., 1987. The shaken baby syndrome: a clinical, pathological, and biomechanical study. J. Neurosurg. 66, 409–415.

Duhaime, A.C., Alario, A.J., Lewander, W.J., Schut, L., Sutton, L.N., Seidl, T.S., Nudelman, S., Budenz, D., Hertle, R., Tsiaras, W., et al., 1992. Head injury in very young children: mechanisms, injury types, and ophthalmologic findings in 100 hospitalized patients younger than 2 years of age. Pediatrics 90 (2 Pt. 1), 179–185.

Eucker, S.A., Smith, C., Ralston, J., Friess, S.H., Margulies, S.S., 2011. Physiological and histopathological responses following closed rotational head injury depend on direction of head motion. Exp. Neurol. 227 (1), 79–88.

Gefen, A., Margulies, S.S., 2004. Are in vivo and in situ brain tissues mechanically similar? J. Biomech. 37 (9), 1339–1352.

Gennarelli, T.A., Thibault, L.E., Adams, J.H., Graham, D.I., Thompson, C.J., Marcincin, R.P., 1982. Diffuse axonal injury and traumatic coma in the primate. Ann. Neurol. 12 (6), 564–574.

Haney, S.B., Starling, S.P., Heisler, K.W., Okwara, L., 2010. Characteristics of falls and risk of injury in children younger than 2 years. Pediatr. Emerg. Care 26 (12), 914–918.

Helfer, R.E., Slovis, T.L., Black, M., 1977. Injuries resulting when small children fall out of bed. Pediatrics 60 (4), 533–535.

Ibrahim, N.G., Margulies, S.S., 2010. Biomechanics of the toddler head during low-height falls: an anthropomorphic dummy analysis. J. Neurosurg. Pediatr. 6 (1), 57–68.

Irwin, A., Mertz, H., 1997. Biomechanical Basis for the CRABI and Hybrid III Child Dummies. SAE Technical Paper 973317.

Luck, J.F., 2012. The Biomechanics of the Perinatal, Neonatal and Pediatric Cervical Spine: Investigation of the Tensile, Bending and Viscoelastic Response Dissertation. Duke University.

Luck, J.F., Nightingale, R.W., Loyd, A.M., Prange, M.T., Dibb, A.T., Song, Y., Fronheiser, L., Myers, B.S., 2008. Tensile mechanical properties of the perinatal and pediatric PMHS osteoligamentous cervical spine. Stapp Car Crash J. 52, 107–134.

Margulies, S.S., Thibault, L.E., 1992. A proposed tolerance criterion for diffuse axonal injury in man. J. Biomech. 25 (8), 917–923.

Mayr, J., Seebacher, U., Schimpl, G., Fiala, F., 1999. Highchair accidents. Acta Paediatr. 88 (3), 319–322.

Melvin, J., 1995. Injury Assessment Reference Values for the CRABI 6-Month Infant Dummy in a Rear-Facing Infant Restraint with Airbag Deployment. SAE Transactions #950872: 1–12.

Monea, A.G., Van der Perre, G., Baeck, K., Delye, H., Verschueren, P., Forausebergher, E., Van Lierde, C., Verpoest, I., Vander Sloten, J., Goffin, J., Depreitere, B., 2014. The relation between mechanical impact parameters and most frequent bicycle related head injuries. J. Mech. Behav. Biomed. Mater. 33, 3–15.

Ommaya, A.K., Goldsmith, W., Thibault, L., 2002. Biomechanics and neuropathology of adult and paediatric head injury. Br. J. Neurosurg. 16 (3), 220–242.

Pellman, E.J., Viano, D.C., Tucker, A.M., Casson, I.R., 2003. Concussion in professional football: location and direction of helmet impacts—part 2. Neurosurgery 53 (6), 1328–1340 discussion 1340–1321.

Prange, M., Coats, B., Duhaime, A.C., Margulies, S., 2003. Anthropomorphic simulations of falls, shakes, and inflicted impacts in infants. J. Neurosurg. 99, 143–150.

Prange, M., Luck, J., Dibb, A., Van Ee, C., Nightingale, R., Myers, B., 2004. Mechanical properties and anthropometry of the human infant head. Stapp Car Crash J. 48, 279–299.

Prange, M.T., Margulies, S.S., 2002. Regional, directional, and age-dependent properties of the brain undergoing large deformation. J. Biomech. Eng. 124 (2), 244–252.

Raghupathi, R., Margulies, S.S., 2002. Traumatic axonal injury after closed head injury in the neonatal pig. J. Neurotrauma 19 (7), 843–853.

Reece, R.M., Sege, R., 2000. Childhood head injuries: accidental or inflicted? Arch. Pediatr. Adolesc. Med. 154 (1), 11–15.

Rowson, S., Duma, S.M., Beckwith, J.G., Chu, J.J., Greenwald, R.M., Crisco, J.J., Brolinson, P.G., Duhaime, A.C., McAllister, T.W., Maerlender, A.C., 2012. Rotational head kinematics in football impacts: an injury risk function for concussion. Ann. Biomed. Eng. 40 (1), 1–13.

Strait, R.T., Siegel, R.M., Shapiro, R.A., 1995. Humeral fractures without obvious etiologies in children less than 3 years of age: when is it abuse? Pediatrics 96 (4 Pt. 1), 667–671.

Sullivan, S., Friess, S.H., Ralston, J., Smith, C., Propert, K.J., Rapp, P.E., Margulies, S.S., 2013. Behavioral deficits and axonal injury persistence after rotational head injury are direction dependent. J. Neurotrauma 30 (7), 538–545.

Tarantino, C.A., Dowd, M.D., Murdock, T.C., 1999. Short vertical falls in infants. Pediatr. Emerg. Care 15 (1), 5–8.

Thompson, A., Bertocci, G., Pierce, M.C., 2013. Assessment of injury potential in pediatric bed fall experiments using an anthropomorphic test device. Accid. Anal. Prev. 50, 16–24.

Thompson, A., Bertocci, G., Rice, W., Pierce, M., 2011. Pediatric short-distance household falls: biomechanics and associated injury severity. Accid. Anal. Prev. 43 (1), 143–150.

Thompson, A.K., Bertocci, G., Pierce, M.C., 2009. Assessment of head injury risk associated with feet-first free falls in 12-month-old children using an anthropomorphic test device. J. Trauma 66 (4), 1019–1029.

Weaver, A.A., Danelson, K.A., Stitzel, J.D., 2012. Modeling brain injury response for rotational velocities of varying directions and magnitudes. Ann. Biomed. Eng. 40 (9), 2005–2018.

Weber, W., 1984. Experimental studies of skull fractures in infants. Z. Rechtsmed. 92 (2), 87–94.

Yoganandan, N., Pintar, F.A., 2004. Biomechanics of temporo-parietal skull fracture. Clin. Biomech. (Bristol, Avon) 19 (3), 225–239.